Hindawi

Research Article

Electron Beam-Initiated Grafting of Methyl Methacrylate on Silicon Nanowires: Investigating Optical and Structural Properties

Muhammad Abdullah Izat Bin Mohd Yassin ⬤,[1] **Khaidzir Hamzah,**[2] **and Sib Krishna Ghoshal**[3]

[1]*Faculty of Bioeconomics and Health Sciences, Universiti Geomatika Malaysia, Kuala Lumpur, Malaysia*
[2]*Faculty of Chemical and Energy Engineering, Universiti Teknologi Malaysia, Johor, Malaysia*
[3]*Department of Physics, Faculty of Science, Universiti Teknologi Malaysia, Johor, Malaysia*

Correspondence should be addressed to Muhammad Abdullah Izat Bin Mohd Yassin; drabdullahizat@geomatika.edu.my

Silicon nanowire (SiNW) is a one-dimensional nanostructured material that had been widely studied due to its potential applications in various fields. Combination of polymers and nanostructured materials offers great potential for enhanced material with many possible applications. The investigation focuses on how this grafting process influences the optical properties of SiNWs, aiming to uncover potential applications for these hybrid materials. This paper comprehensively presents the methodology and characterization of these SiNWs-MMA hybrid materials, exploring their potential applications. The experimental process begins with the preparation of six SiNWs using RF magnetron sputtering, involving the deposition of an Au catalyst and subsequent growth of SiNWs. The radiation-induced grafting involves exposing SiNWs to electron beams and subsequently grafting MMA onto the surface. The outcomes reveal that the grafting percentage of MMA onto SiNWs increases with higher radiation doses, leading to a polymer layer covering the SiNWs. This grafting is confirmed through Fourier-transform infrared (FTIR) spectroscopy, which shows characteristic peaks of MMA on the surface. X-ray diffraction (XRD) analysis demonstrates changes in crystallite size, microstrain, and dislocation density upon grafting, which are attributed to stress relief and the effect of polymer on SiNWs' lattice. Field emission scanning electron microscopy (FESEM) images exhibit the increasing MMA layer on SiNWs as the grafting percentage increases. UV-visible spectroscopy shows that the introduction of MMA increases the optical band gap of SiNWs, attributed to changes in surface roughness due to the carbon from MMA. This study introduces a novel method of hybridizing SiNWs with MMA through radiation-induced grafting. The detailed characterization of the resulting SiNWs-MMA hybrid materials sheds light on their structural and optical properties. These findings hold the promise of innovative applications in various technological fields, further advancing nanotechnology.

1. Introduction

One-dimensional nanostructured materials have revolutionized the technological landscape and have been extensively studied since the discovery of carbon nanotubes. Apart from carbon nanotubes, various other nanostructured materials have been reported, such as Cu_2O nanowires exhibiting efficient charge carrier separation and remarkable visible light photoresponse and copper-based metal oxides for chemiresistive gas sensors [1]. However, one of the most significant nanostructured materials is silicon nanowires (SiNWs) due to their widespread implementation in semiconductors, electronics, solar cells, sensors, and lithium batteries. SiNWs offer a promising array of applications, primarily due to their large surface-to-volume ratio, which renders electrical transport highly sensitive to the nanowire's surface condition [2, 3]. Moreover, SiNWs demonstrate unique piezoresistance properties, and their size and shape can be manipulated via surface modification to unlock their full potential [4]. These attributes surpass those of bulk

silicon, where electrical conductivity is typically controlled by the inclusion of dopants. However, excessive doping can cause mobility degradation due to variations in the local electrostatic potential arising from the positioning of the doping atoms in the nanowires [5].

Despite the advantages of SiNWs, their high surface-to-volume ratio also brings about a significant number of outer shell defect states, which may compromise the material's performance [6]. In addition, the easy adsorption of molecules on the SiNWs' surface can lead to uncontrollable influences on conductivity [7]. To mitigate these challenges, surface passivation has conventionally been employed to reduce surface defects. Nevertheless, recent studies have revealed that surface passivation can also impact other characteristics of SiNWs, such as carrier mobility, via the thermal growth of SiO_2 [8, 9]. Furthermore, chemical treatment of SiNW surfaces with organic compounds has shown potential for trap reduction and surface passivation [10]. Another promising avenue involves the coating of SiNWs with materials such as diamond and gold, leading to significant improvements in their thermal and electrical properties [11, 12].

One notable technique that offers numerous advantages, including simplicity, precise parameter control, uniform grafting of monomers at low temperatures, flexibility, and reproducibility, is radiation-induced grafting. Previous research has investigated hybrid SiNWs-polymer composites, such as polyacrylic acid, poly (3,4-ethylene-dioxythiophene), and poly methyl methacrylate (MMA). Notably, MMA-coated SiNWs demonstrated a hydrophilic SiNW core with a hydrophobic polymer shell on the surface [13]. However, to date, no study has reported on the hybridization of SiNWs and polymers using the radiation-induced grafting approach. This study aims to introduce a novel method of material hybridization, employing radiation-induced grafting. We anticipate that investigating the structural and optical properties of these hybrid materials will yield valuable insights into the grafting capability of SiNWs and MMA, along with the potential applications of this unique combination.

In this paper, we present the detailed methodology for the radiation-induced grafting process and the characterization of the resulting SiNWs-MMA hybrid material. In addition, we discuss the structural, optical, and surface properties of the hybrid material and explore its potential applications in various technological fields. The findings from this study could significantly contribute to the advancement of nanotechnology and pave the way for innovative applications of SiNWs and polymers in diverse industries.

2. Materials and Methods

2.1. Silicon Nanowire Preparation. The deposition of SiNWs (silicon nanowires) began with the precise cutting of an ultraflat Si wafer {100} into smaller $1\,cm \times 1\,cm$ wafers. These smaller wafers were then thoroughly cleaned in an ultrasonic bath to ensure a pristine surface. To eliminate any native oxide layers, the prepared samples underwent a 10-minute immersion in an HF solution. The deposition of the Au catalyst was carried out using RF magnetron sputtering within a vacuumed chamber operating at a pressure of 1.5×10^{-5} torr. The successful deposition of the Au catalyst involved introducing argon gas at a flow rate of 130 sccm and applying an RF power of 50 W for 30 seconds. Subsequently, the Au thin film was annealed at 600°C for 30 minutes to facilitate the formation of Au droplets, which served as the catalyst for SiNW growth. The SiNW growth process utilized the same magnetron sputtering system. After annealing the Au catalyst at 600°C for 30 minutes, the Au target was replaced with a Si target. Prior to SiNW deposition, the chamber was once again evacuated to 1.5×10^{-5} torr. The deposition of SiNWs was achieved by introducing argon at 130 sccm with an RF power of 100 W for 120 minutes, while maintaining a temperature of 600°C.

2.2. Methyl Methacrylate Cover. The SiNWs samples were initially weighed to determine their initial weight. Subsequently, each SiNW was placed inside an individual zip-lock plastic bag and purged with nitrogen gas to eliminate any oxide and undesired elements. The samples were then subjected to irradiation using electron beams at varying doses of 10 kGy, 30 kGy, 50 kGy, 70 kGy, and 90 kGy, while keeping other parameters constant, such as a beam energy of 2 MeV, a pulse current of 3 mA, and a dose rate of 10 kGy per path. Following irradiation, the samples were stored in dry ice until the subsequent steps of the experiment.

Meanwhile, a monomer solution was prepared by combining 89% of MMA (99% purity, Sigma-Aldrich, Missouri), 1% of tween 20 (Sigma-Aldrich, Missouri), and 10% of distilled water. Tween 20, a polysorbate-type nonionic surfactant, served as an emulsifier to dissolve the hydrophobic substance. The mixture was stirred using a magnetic stirrer for 10 minutes initially and then for an additional 15 minutes to ensure thorough homogeneity. The monomer mixture was subsequently transferred into a glass ampoule and purged with nitrogen gas for 30 minutes. An overview of these procedures is provided in Figure 1.

Once both samples and monomer had successfully prepared, the grafting procedure is now ready to be executed. The grafting procedure was initiated by carefully transferring the sample cylinder from the vacuum pump and connecting it to the monomer-filled cylinder. It was imperative to maintain the vacuum condition within the cylinder during this transfer (see Figure 2(a)). Following the secure connection, the monomer (50 ml) was introduced into the sample cylinder without disrupting the vacuum state. The entire setup was then placed in a water bath at a controlled temperature of 40°C to facilitate the grafting process, allowing it to proceed for a duration of 2 hours (see Figure 2(b)). Once the grafting period elapsed, the sample was taken out of the cylinder and subsequently cleansed with distilled water to eliminate any residual MMA (see Figure 2(c)). After the cleansing step, the sample was carefully weighed to determine its final weight (see Figure 2(d)).
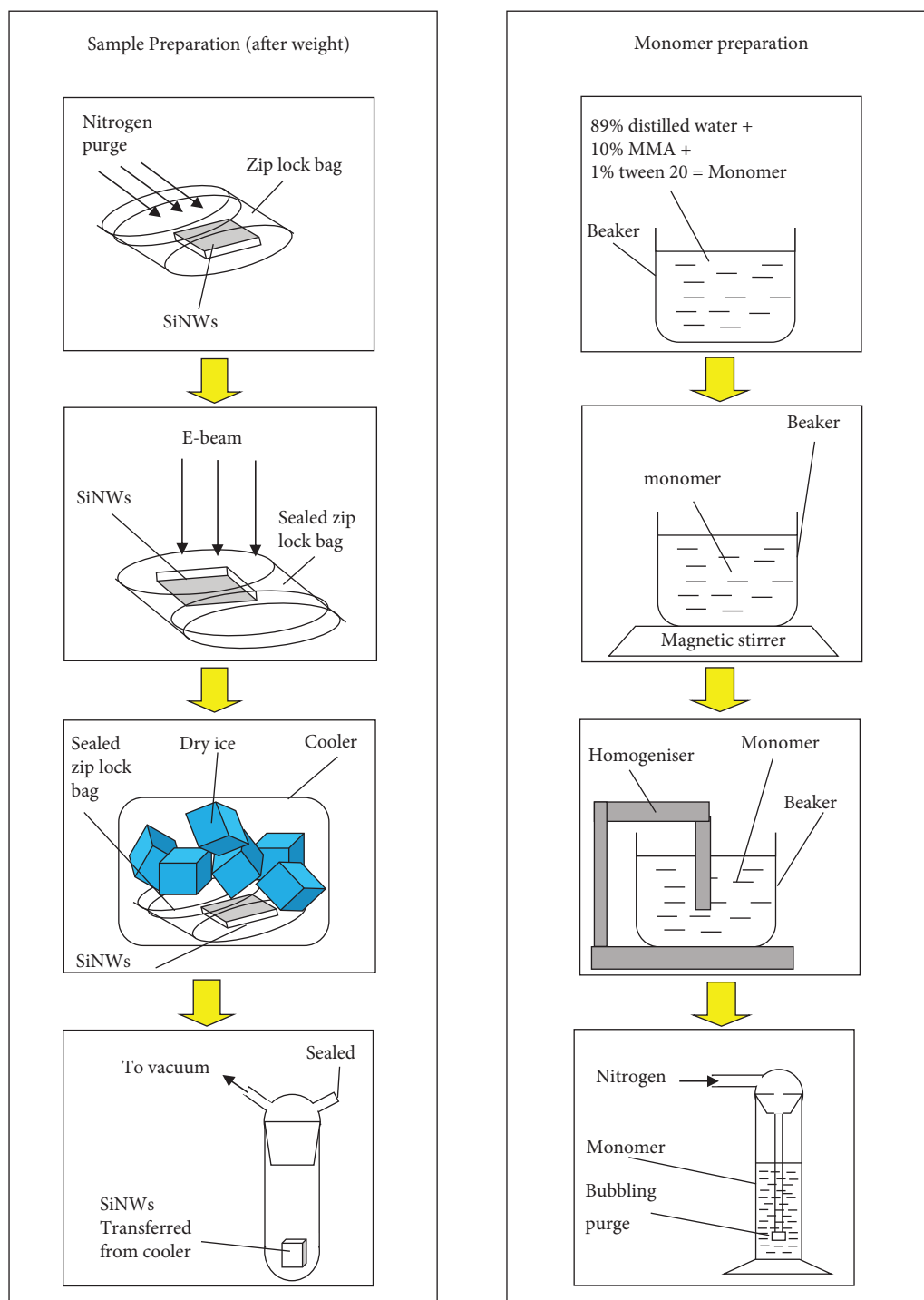
FIGURE 1: Preparation of sample and monomer before grafting process.

The grafting parameters conducted on samples are presented in Table 1. One of the samples (S1) was not grafted to facilitate comparison of the grafted and ungrafted samples during analysis.

2.3. Material Characterization. The X-ray diffraction (XRD) analysis was conducted using a Bruker D8-advance X-ray diffractometer with Cu-Kα radiation ($\lambda = 1.54060$ Å). The 2θ range for data collection was set from $10°$ to $80°$, and each step had a counting time of 0.4 s. The samples were further subjected to analysis using a Perkin Elmer Frontier NIR-FTIR spectrometer equipped with ATR polarization accessories. FT-IR spectra were acquired by recording 64 scans within the wavenumber range of 650 cm^{-1}–4000 cm^{-1}, employing transmittance mode. For morphological investigation, a high-resolution two-beam scanning electron microscope with the Schottky cathode Zeiss CrossBeam 340
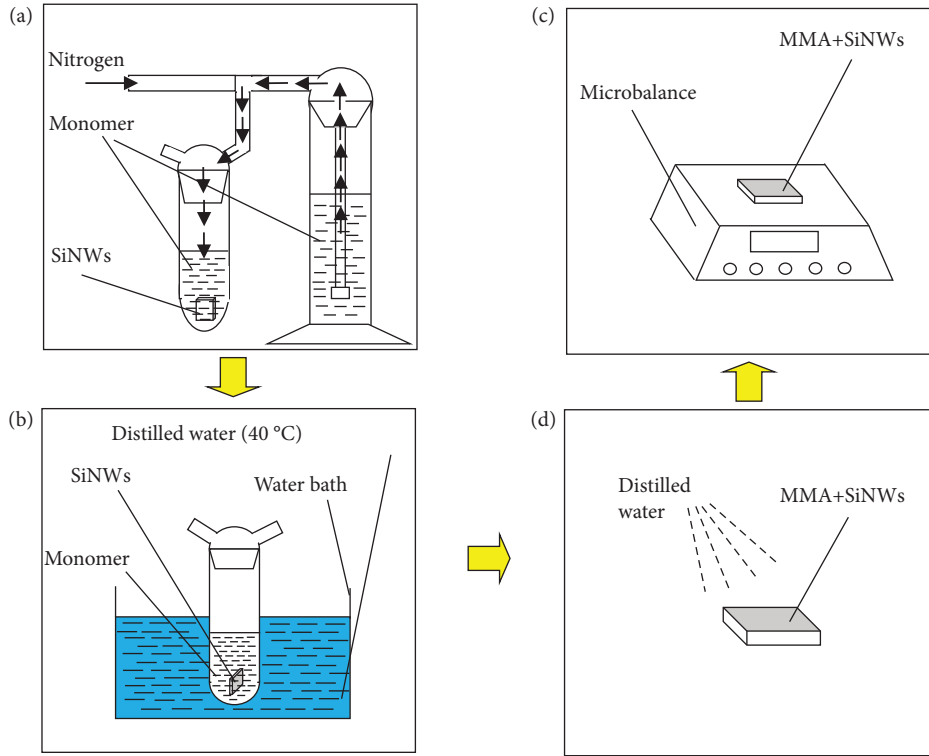
FIGURE 2: Procedure of radiation-induced grafting.

TABLE 1: Grafting parameters.

Samples	Dose (kGy)	Grafting time (hr)	Grafting temperature (°C)
S1	—	—	—
S2	10	2	40
S3	30	2	40
S4	50	2	40
S5	70	2	40
S6	90	2	40

(Germany) was utilized. Optical reflectance spectra were measured in the wavelength range of 800–1650 nm, employing a UV-Vis-NIR spectrophotometer (Shimadzu, model UV3600 plus).

3. Results and Discussion

3.1. MMA Covered. After performing the radiation-induced grafting on the samples, the grafting percentage of weighed samples was calculated using equation (1) and the result is shown in Figure 3.

$$\text{grafting\%} = \left(\frac{W_g - W_0}{W_0}\right) \times 100. \tag{1}$$

Figure 3 illustrates the relationship between the grafting percentage and the radiation dose applied to the samples. The data presented in the graph indicate a direct proportionality, as the grafting percentage increases from 0.20% to 0.35% with higher radiation doses [14]. The polymerization system's radiation dose plays a crucial role in

significantly enhancing the degree of grafting or the grafting percentage. The observed increase in sample weight suggests the presence of grafted poly MMA on the sample surface. The initial sample weight refers to the weight of SiNWs before the grafting process took place. Subsequent changes in weight after the grafting procedure indicate that the additional weight can be attributed to MMA. This successful grafting process is further supported by consistent findings from other studies that report a linear increase in grafting percentage with rising radiation doses. Specifically, grafting percentages of 0.20%, 0.23%, 0.27%, 0.31%, and 0.35% were achieved with radiation doses of 10 kGy, 30 kGy, 50 kGy, 70 kGy, and 90 kGy, respectively [15]. The electron beam irradiation at higher levels contributes to the cleavage of covalent bonds in the silicon molecular structure, leading to increased radical formation that facilitates MMA grafting [14, 16, 17].

3.2. FTIR Analysis. FTIR transmittance analysis was utilized to characterize the surface composition of the samples. The outcomes of this analysis are illustrated in Figure 4.

Figure 4 illustrates the diverse bonding characteristics observed on the as-prepared SiNWs. In the lower wavenumber range ($800 \, \text{cm}^{-1}$ to $1500 \, \text{cm}^{-1}$), distinct peaks corresponding to Si-O bonds are evident at $845 \, \text{cm}^{-1}$, $1169 \, \text{cm}^{-1}$, and $1259 \, \text{cm}^{-1}$. The peak at $845 \, \text{cm}^{-1}$ corresponds to the stretching of Si-O bonding [18], while the signals at $1165 \, \text{cm}^{-1}$ and $1240 \, \text{cm}^{-1}$ are associated with the stretching and symmetrical and antisymmetrical vibrational modes of the Si-O-Si bridges in SiO_x [19]. In addition,

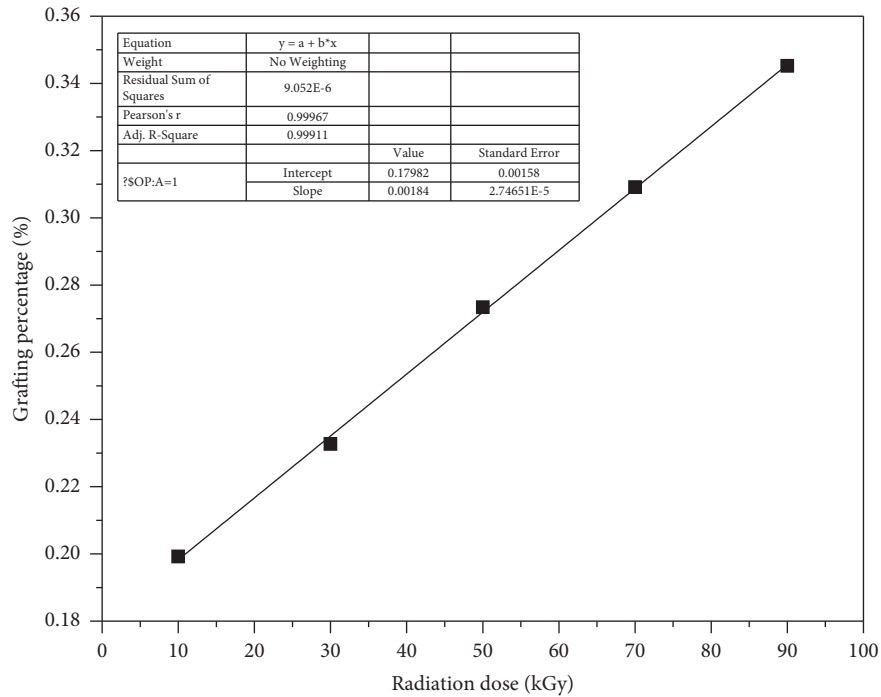| Equation	y = a + b*x		
Weight	No Weighting		
Residual Sum of Squares	9.052E-6		
Pearson's r	0.99967		
Adj. R-Square	0.99911		
		Value	Standard Error
?$OP:A=1	Intercept	0.17982	0.00158
	Slope	0.00184	2.74651E-5

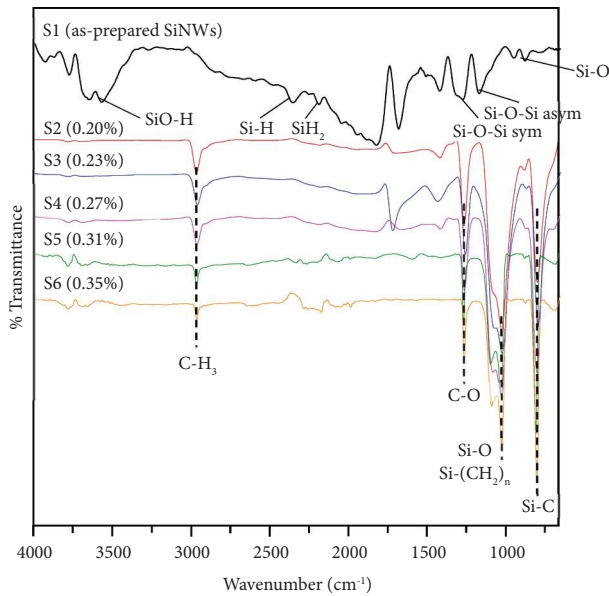FIGURE 3: Influence of radiation dose on the grafting percentage.

FIGURE 4: ATR-FTIR spectra of samples before and after grafting.

characteristic transmittance peaks arising from various vibration modes of the SiH_x bond are also identified. Specifically, the peaks at $2205\,cm^{-1}$ correspond to the wagging and stretching vibration modes of the Si-H bond, whereas the peaks at $2186\,cm^{-1}$ represent the wagging, scissors, and stretch vibration modes of the $Si-H_2$ bond. These observed peaks are directly related to the hydrogen signature present at the SiNW surface [20]. The presence of a broad band between $3573\,cm^{-1}$ and $3657\,cm^{-1}$ is attributed to the stretching signal of the SiO-H bond [20].

Subsequent to the grafting of MMA onto the SiNWs, the spectra reveal several new transmittance peaks, indicating the presence of MMA on the surface. These peaks are clearly evident at wavenumbers of $800\,cm^{-1}$, $1020\,cm^{-1}$, $1257\,cm^{-1}$, and $2963\,cm^{-1}$. The peak at $800\,cm^{-1}$ indicates the presence of an σ-bonded SiC matrix, while the peak at $1020\,cm^{-1}$ is assigned to the $Si-CH_3$ rocking or wagging mode and the Si-O stretching vibration [21], thereby confirming the grafting of methyl methacrylate onto the SiNWs. Moreover, the peak at $2963\,cm^{-1}$ is attributed to the asymmetric stretching ($v$as) and symmetric (vs) vibrations of methyl (CH_3) groups, and the shoulder around $1257\,cm^{-1}$ is attributed to the stretching vibration modes of C-O (ester bond) [22, 23]. These peaks further confirm the successful grafting of MMA on the surface of the samples.

3.3. X-Ray Diffraction. The X-ray diffraction (XRD) analysis was done to investigate the crystalline structure of the samples. The XRD pattern obtained is shown in Figure 5. The XRD pattern in the figure shows the silicon diffraction peak at $2\theta = 45°$ (200), which is commonly observed for SiNWs. This peak is also observed on the samples after MMA is grafted on them. The sharp and narrow diffraction peaks indicate that the SiNWs has good crystallinity [24]. However, as the radiation grafting was applied on the samples, the peak at $2\theta = 45°$ is observed to reduce its intensity. This phenomenon is due to the distinct scattering behavior of the MMA's amorphous layer, stemming from its disordered atomic arrangement, ordered crystalline lattice of SiNWs. This difference in scattering efficiencies results in the observed decrease in peak intensity [25].
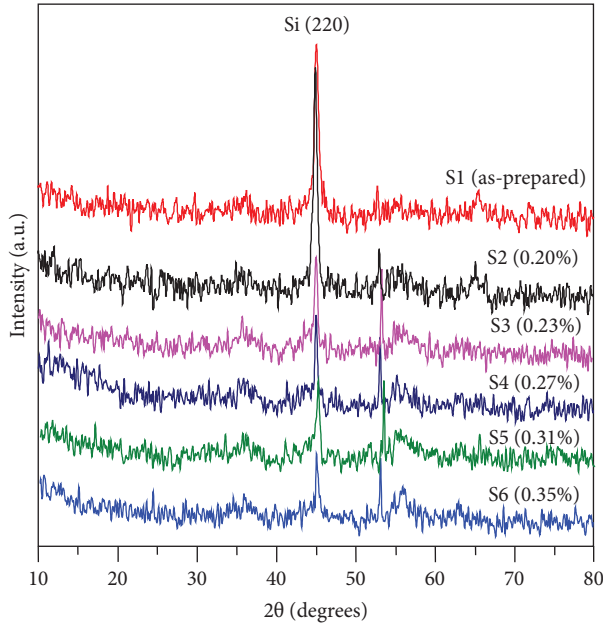
Figure 5: XRD pattern of samples.

The crystalline size size of SiNWs was calculated by the following Scherrer equation [26]:

$$D = \frac{0.94\lambda}{\beta \cos\Theta},\qquad(2)$$

where D is the crystallite size (average), θ is the diffraction angle, λ is the wavelength (0.154 nm) of radiation used for the diffraction, and β is the full-width at half maximum (FWHM) of the observed peaks. The dislocation density (δ) was calculated from Williamson and Smallman's formula [27].

$$\delta = \frac{1}{D^2}.\qquad(3)$$

Peak broadening in X-ray diffraction (XRD) is caused by deviations from the ideal crystalline structure within a material. Peak broadening is caused by a variety of factors, including changes in solution conditions, fluctuations in crystallite size, and the existence of microstrain. Among these underlying reasons, microstrain (ε) stands out as a particularly significant contributor to the observed peak broadening phenomena. The following equation expresses the measurement of microstrain:

$$\varepsilon = \frac{\beta}{4\tan\Theta},\qquad(4)$$

where ε = microstrain, β = FWHM, and θ = diffraction angle or Bragg's angle. The microstrain and dislocation density are summarized in Table 2.

The findings presented in Table 2 demonstrate that the initial as-prepared SiNWs exhibit a crystallite size of 12.98 nm, with a microstrain of 7.28×10^{-3} and a dislocation density of 5.94×10^{-3}. Upon introduction of MMA on the SiNWs surface, a notable enhancement in crystallite size to 28.86 nm is observed, concomitant with a reduction

in microstrain and dislocation density to 3.28×10^{-3} and 1.20×10^{-3}, respectively. The observed phenomenon can be attributed to the stress relief induced on the nanowires' surface by the introduction of MMA due to differences in thermal expansion coefficients between MMA and silicon, which lead to a reduction in microstrain and stress within the nanowires' crystalline lattice [28]. Subsequently, as the grafting percentage of MMA increases to 0.23%, 0.27%, 0.31%, and 0.35%, a discernible reduction in crystallite size to 26.69 nm, 20.59 nm, 19.26 nm, and 16.34 nm, respectively, is noted. Notably, a complementary trend is observed, wherein a decrease in crystallite size correlates with an increment in dislocation density, as detailed in Table 2. This trend can be attributed to the increase in the occurrence of grain boundaries because of a decrease in crystallite size. As the grafting percentage of MMA increases, the strain imposed on the nanowire caused by difference in mechanical properties is not effectively relieved. The polymer matrix acts as a constraint, preventing the nanowire from fully relaxing its elastic strain. This can lead to a higher density of dislocations forming within the nanowire [28]. The decrease in the lattice parameter can also be attributed to the lattice vacancies generated subsequent to the application of electron beam dosage during the grafting procedure. This phenomenon leads to distortion and divergence from the cubic spinel structure. Furthermore, the electron beam conventionally induces compressive strain, thereby introducing disorder within the lattice configuration of SiNWs (silicon nanowires). Consequently, this alteration culminates in an increase of the grafting percentage of MMA, as shown in Figure 3 [29, 30].

3.4. FESEM Images. Figure 6(a) shows that the Si was in the form of a nanowire. This formation occurred due to the VLS mechanism that happened during the sputtering process [31]. In this mechanism, the Au is first deposited on the substrate. As the temperature was raised to 600°C, the Si deposition was carried out. At this temperature, small Au-Si alloy droplets are formed. The continuous deposition of Si particles on the sample during this process leads to the supersaturation of Si on the substrate. Eventually, the Si freezes out at the Si/droplet interface and finally leads to the formation of SiNWs [32, 33].

Following the radiation grafting procedure, subsequent FESEM imaging was conducted on the samples to investigate the microscopic visual impact of grafting. Figure 6 delineates the progressive changes in surface morphological features in response to varying grafting percentages. Notably, the visibility of silicon nanowires (SiNWs) diminishes gradually with escalating grafting percentages, attributed to the surface coverage of methyl methacrylate (MMA) postgrafting. In Figure 6(b), where the grafting percentage is at its lowest (0.20%), the Si nanostructure's visual characteristics slightly change compared to the samples before MMA was grafted, where the rough, clod-like Si became smoother. Advancing to a grafting percentage of 0.31%, Figure 6(c) shows

TABLE 2: Summarized microstructural and elastic parameters of the samples.

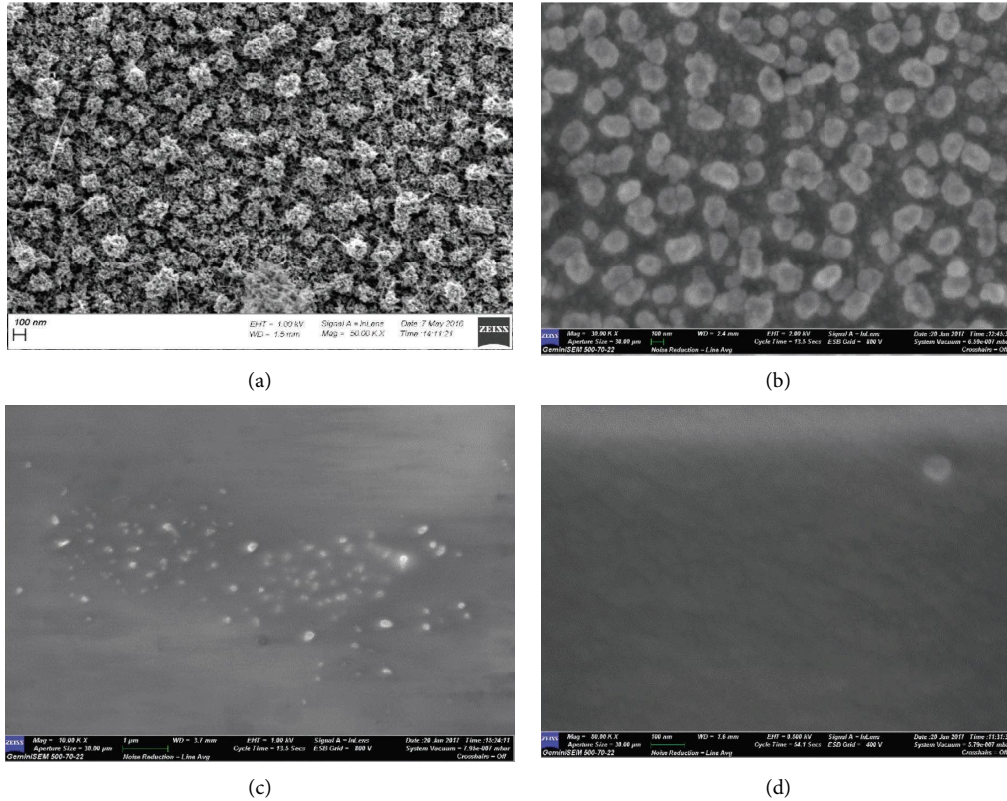| Grafting percentage (%)	Peak position	FWHM	Crystallite size, D (nm)	Microstrain, ε ($\times 10^{-3}$)	Dislocation density, ε ($\times 10^{-3}$)
Ungrafted	45.07	0.69	12.98	7.28	5.94
0.2	45.04	0.31	28.86	3.28	1.20
0.23	45.04	0.34	26.69	3.54	1.40
0.27	45.08	0.44	20.59	4.59	2.36
0.31	45.08	0.47	19.26	4.90	2.70
0.35	45.04	0.55	16.34	5.79	3.75

(a)

(b)

(c)

(d)

FIGURE 6: FESEM image of (a) as-prepared sample and (b) 0.20%, (c) 0.31%, and (d) 0.35% grafting percentage.

a perceptible increase in surface smoothness, and the SiNWs manifest as smaller bumps on the surface. Figure 6(d) portrays the culmination of this trend, wherein the surface achieves complete smoothness at a grafting percentage of 0.35%. This evolution signifies the augmenting deposition of MMA onto the sample surface, consequent to elevated grafting percentages. Evidently, the observed correlation reveals that as grafting percentages escalate, the MMA layer thickness experiences a corresponding increase.

The escalating thickness of MMA (methyl methacrylate) can be attributed to the dosage of radiation applied to the specimen. A reduction in radiation dosage would lead to a decrease in grafting efficiency. This scenario would result in a diminished generation of free radicals in the Si (silicon) substrate, consequently yielding a reduced initiation of copolymerization between Si and MMA, as indicated by previous investigations [34].

3.5. UV-Visible Spectroscopy.

UV-vis spectroscopy analysis was conducted to explore alterations in the optical properties of SiNWs through the grafting of MMA. The UV-vis spectroscopy results for both the as-prepared SiNWs and the SiNWs post-MMA grafting are depicted in Figure 7.

Figure 7 depicts the reflectance spectra of the SiNWs samples prior to the grafting of MMA onto them. The figure illustrates that the as-prepared SiNWs sample exhibits notably low reflectance, particularly in the wavelength range below 1050 nm, ranging from 9% to 21%. This property was observed due to the strong light scattering, which results in partial localization of the excitation light in SiNW [35]. The diminished reflectance in the near-infrared (near-IR) region indicates the high sensitivity of SiNWs to visible and near-IR radiation [36]. Following the grafting of MMA onto the samples, it can be generally observed that the inclusion of MMA
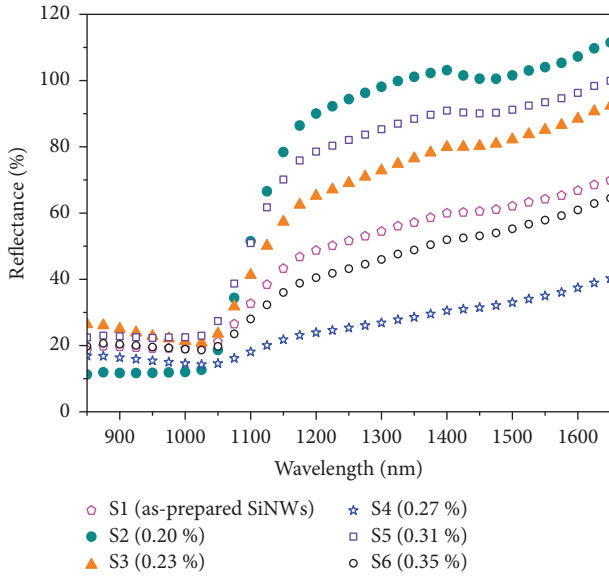
FIGURE 7: UV-vis spectroscopy of SiNWs before and after MMA radiation grafting.

increases the reflectance of the SiNWs samples. Although the increase in reflectance was not very high (11% for samples with a grafting percentage of 0.35%), the result did show that the grafted MMA on the samples did affect the optical characteristics of the SiNWs. Notably, in the shorter wavelength range from 850 nm to 950 nm, the reflectance experiences increment with rising grafting percentages. At a grafting percentage of 0.31%, a reflective increase from 18% to 22% (a 4% increment) is observed. Furthermore, as the grafting percentage reaches 0.35%, the reflectance rises from 8% to 19% (an 11% increment). The increasing reflectance phenomenon indicates the decreasing transparency of the samples. This phenomenon is due to the contribution of carbon and oxygen in the MMA in the samples. As the MMA is grafted on the samples, the roughness of the SiNWs surface decreases due to the contribution of carbon, hydrogen, and oxygen fractions from the smooth surface of the MMA on the top of the sample, which is supported by the FTIR spectra in Figure 4 and FESEM images in Figure 6. As the grafting percentage of the samples increases, the surface becomes smoother, which can also be seen in the FESEM image in Figure 6, which leads to an increase in the reflection coefficient in the near-IR region [36].

All of the reflectance spectra in the near-infrared region seem to be stable. The stable and reflectance of UV-vis NIR spectra indicates that the samples are very sensitive to the visible to near-IR radiation. This wavelength is known to be very essential to photosensitive device applications [36].

The optical band gap of the sample was calculated using the Tauc formula (equations (5)–(7)), and from the calculation, a graph of $(h\nu\alpha)^{(1/2)}$ against $h\nu$ was constructed to determine the optical band gap of the sample. The graph is presented in Figure 8.
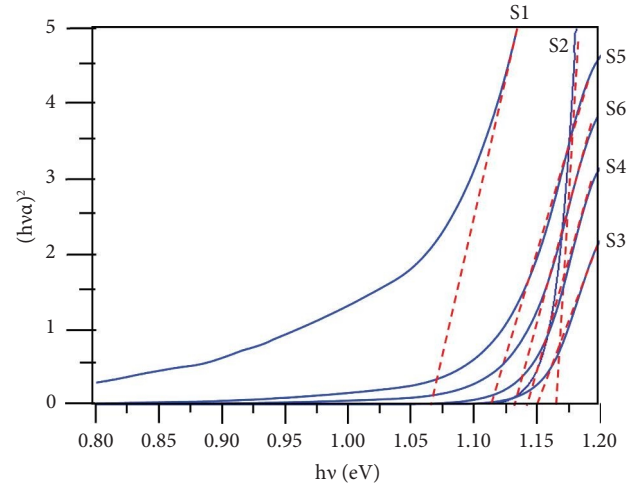

FIGURE 8: Tauc plot of samples before and after MMA radiation grafting.

$$(\alpha h\nu)^2 = A\left(h\nu - E_g\right), \qquad (5)$$

$$\alpha = 2.303 \log\left(\frac{T}{d}\right), \qquad (6)$$

$$A = \log T. \qquad (7)$$

Figure 8 is the Tauc plot of SiNWs before and after MMA was grafted on them, with the variation in grafting percentage. In the figure, the optical band gap, E_g, was estimated by taking the intercept of the extrapolation to zero absorption with the photon energy axis. The result is presented in Table 3.

The findings outlined in Table 3 reveal an increasing trend wherein the introduction of MMA grafting onto the samples led to a notable increase in their optical band gap. Initially, the as-synthesized SiNWs exhibited an optical band gap of 1.07 eV, which subsequently elevated to 1.17 eV upon grafting of MMA at a rate of 0.20%. In contrast, with a grafting percentage of 0.23%, followed by a marginal increase to 0.27%, the optical band gap experienced a reduction to 1.15 eV and 1.14 eV, respectively. Continuing this trend, a successive decline in the optical band gap was observed; the samples' band gap values dwindled further to 1.13 eV and 1.12 eV as the grafting percentages reached 0.31% and 0.35%, respectively. These outcomes are presented graphically in Figure 9. This graphical representation serves as a visual aid to facilitate an in-depth examination of the influence exerted by varying MMA grafting percentages on the band gap of SiNWs, contributing to a more comprehensive understanding of the observed phenomenon.

Figure 9 shows that as the MMA was introduced on the surface of the SiNWs, the optical band gap of the samples increased significantly. The increasing optical energy band gap following the incorporation of MMA onto the sample, particularly evident at a grafting percentage of 0.20%, is attributed to the presence of carbon stemming from the

TABLE 3: Influence of MMA grafting percentage on the band gap.

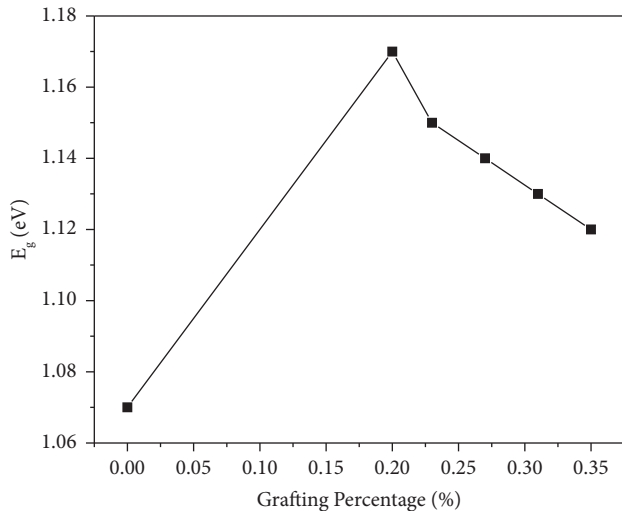| Grafting percentage (%)	Optical band gap (eV)
0	1.07
0.20	1.17
0.23	1.15
0.27	1.14
0.31	1.13
0.35	1.12

FIGURE 9: Graph of energy band gap against grafting percentage of samples.

MMA. This carbon incorporation results in a reduction of the sample's transparency, a phenomenon expounded upon and visually depicted in Figure 6.

However, the depicted figure also reveals a contrary pattern, as the band gap demonstrates a diminishing tendency with escalating grafting percentages. The reduction in the energy band gap values was caused by the addition of MMA thickness, which is shown by the loss of visibility of SiNWs in Figures 6(b)–6(d). The discrepancies in PMMA molecular weight are the likely reason for the minor deviations. It can be implied from the reduction in optical band gap energy that the electronic structure of SiNWs molecules suffers modifications when MMA is added and defects developing in the PMMA matrix may be the determinants of those modifications [37, 38]. This can also be seen and proven by the increasing microstrain and dislocation density presented in the XRD analysis in Table 2. The decreasing transparency of the samples after radiation grafting was due to the decreasing spin density at the film, which is related to the breaking of bonds, which is stronger at the more opaque film. A decrease in transparency also implies an increase in the energy band gap. This means more energy is required to pass through the materials. Therefore, there is a decrease in transparency at this part of the film, which leads to an increase in the energy band gap of the samples with grafted MMA [39]. Materials with larger band gaps generally absorb and emit shorter

wavelength (higher energy photons, which make them a suitable choice of photosensitive material for photon detection) [40].

Before the MMA was grafted on the samples, the film was considered a one-dimensional confined system. In such a one-dimensional system, elementary excitations will experience quantum confinement, resulting in finite motion in the confinement direction and infinite motion in the other two directions [41]. It has been well known that as the confining dimension decreases, typically at the nanoscale, the energy spectrum turns discrete, and thus the band gap of a semiconductor becomes size-dependent. For one-dimensional confinement, the quantization energies increase when the size along the confinement direction decreases [42].

4. Conclusions

SiNWs thin film sample had been successfully synthesized using magnetron sputtering at 600°C for 120 min, with plasma generated at 100 W of power. Radiation-induced grafting of MMA was carried out on the surface of the samples with different radiation doses of 10 kGy, 30 kGy, 50 kGy, 70 kGy, and 90 kGy. It was found that the grafting percentage increased as the radiation dose increased, which is an expected phenomenon in radiation grafting. The grafting percentage of MMA on the SiNWs increased linearly with the increasing radiation dose, where the grafting percentage was 0.20% for 10 kGy, 0.23% for 30 kGy, 0.27% for 50 kGy, 0.31% for 70 kGy, and 0.35% for 90 kGy. The FTIR result shows the success of grafting by the existence of peaks that attribute to SiC, $SiCH_3$, and CH_3 bonds, which can also be visually observed by the FESEM images. The XRD analysis demonstrates the increase in crystallite size and depletion microstrain and dislocation density upon grafting, which are attributed to stress relief and the effect of polymer on SiNWs' lattice. However, the crystallite size decreases to 26.69 nm, 20.59 nm, 19.26 nm, and 16.34 nm as the grafting percentage increases due to the unrelieved strain imposed on the nanowire by MMA. The UV-vis spectroscopy for the samples before MMA was grafted on the surface showed low reflectance below 1050 nm of wavelength, indicating high sensitivity of the samples to visible and near-IR radiation. The UV-vis spectra showed that the grafting of MMA on the samples led to a decrease in transparency. The reflectance spectra indicate that the samples were very sensitive to visible and near-IR radiation. The Tauc plot showed a significant increment in the band gap as MMA was introduced on the SiNWs. The increase in the energy band gap from 1.07 eV for the ungrafted sample to 1.14 eV was also due to the presence of carbon, which caused the samples to lose their transparency. The optical characterizations showed that the MMA-grafted SiNWs did not strongly affect the band gap, and the stable absorption in the NIR region still gave this material great potential for use in photovoltaic, photonics, and photosensitive device applications.

Data Availability

The data and results analysed during the current study are available from the corresponding author upon reasonable request.

Conflicts of Interest

The authors declare that they have no conflicts of interest.

Acknowledgments

References

[1] T. Zhou, Z. Zang, J. wei et al., "Efficient charge carrier separation and excellent visible light photoresponse in Cu_2O nanowires," *Nano Energy*, vol. 50, pp. 118–125, 2018.

[2] A. Tilke, R. H. Blick, H. Lorenz, and J. P. Kotthaus, "Single-electron tunneling in highly doped silicon nanowires in a dual-gate configuration," *Journal of Applied Physics*, vol. 89, no. 12, pp. 8159–8162, 2001.

[3] Y. Cui, Z. Zhong, D. Wang, W. U. Wang, and C. M. Lieber, "High performance silicon nanowire field effect transistors," *Nano Letters*, vol. 3, no. 2, pp. 149–152, 2003.

[4] M. Shao, D. Ma, and S. T. Lee, "Silicon nanowires-synthesis, properties, and applications," *European Journal of Inorganic Chemistry*, vol. 2010, no. 27, pp. 4264–4278, 2010.

[5] A. Asenov, "Random dopant induced threshold voltage lowering and fluctuations in sub-0.1 μm MOSFET's: a 3-D "atomistic" simulation study," *IEEE Transactions on Electron Devices*, vol. 45, no. 12, pp. 2505–2513, 1998.

[6] L. Wei, F. Li, S. Pang, Y. Wang, J. Guo, and J. Chen, "First-principles study of polymer-passivated silicon nanowire outer-shell defects," *Physical Chemistry Chemical Physics*, vol. 24, no. 18, pp. 11169–11174, 2022.

[7] K. Fobelets, P. Ding, N. Mohseni Kiasari, and Z. Durrani, "Electrical transport in polymer-covered silicon nanowires," *IEEE Transactions on Nanotechnology*, vol. 11, no. 4, pp. 661–665, 2012.

[8] J. Jie, W. Zhang, K. Peng, G. Yuan, C. S. Lee, and S. T. Lee, "Surface dominated transport properties of silicon nanowires," *Advanced Functional Materials*, vol. 18, no. 20, pp. 3251–3257, 2008.

[9] K. Seo, S. Sharma, A. A. Yasseri, D. R. Stewart, and T. I. Kamins, "Surface charge density of unpassivated and passivated metal-catalyzed silicon nanowires," *Electrochemical and Solid-State Letters*, vol. 9, no. 3, pp. G69–G72, 2006.

[10] M. Nolan, S. O'Callaghan, G. Fagas, J. C. Greer, and T. F. Frauenheim, "Silicon nanowire band gap modification," *Nano Letters*, vol. 7, no. 1, pp. 34–38, 2007.

[11] V. A. Fonoberov and A. A. Balandin, "Giant enhancement of the carrier mobility in silicon nanowires with diamond coating," *Nano Letters*, vol. 6, no. 11, pp. 2442–2446, 2006.

[12] E. P. Pokatilov, D. L. Nika, and A. A. Balandin, "Acoustic phonon engineering in coated cylindrical nanowires," *Superlattices and Microstructures*, vol. 38, no. 3, pp. 168–183, 2005.

[13] M. J. Mulvihill, B. L. Rupert, R. He, A. Hochbaum, J. Arnold, and P. Yang, "Synthesis of bifunctional polymer nanotubes from silicon nanowire templates via atom transfer radical polymerization," *Journal of the American Chemical Society*, vol. 127, no. 46, pp. 16040-16041, 2005.

[14] J. Lu, M. Yi, J. Li, and H. Ha, "Preirradiation grafting polymerization of DMAEMA onto cellulose fabrics," *Journal of Applied Sciences*, vol. 81, pp. 3578–3581, 2001.

[15] M. M. El-Toony, "Grafting of styrene/methacrylic acid onto a commercial poly (tetraflouroethylene) film for a proton exchange membrane fuel cell," *Arab Journal of Nuclear Science an Applications*, vol. 50, no. 2, pp. 193–208, 2017.

[16] J. E. Wilson and M. Burton, "Radiation Chemistry of monomers, polymers, and plastics," *Physics Today*, vol. 27, no. 7, pp. 50-51, 1974.

[17] H. Magana, C. D. Becerra, A. Serrano-Medina et al., "Radiation grafting of a polymeric prodrug onto silicone rubber for potential medical/surgical procedures," *Polymers*, vol. 12, no. 6, p. 1297, 2020.

[18] B. D. Mistry, *Handbook of Spectroscopic Data Chemistry*, Oxford Book Company, Oxford, UK, 2009.

[19] V. A. Sivakov, F. Voigt, A. Berger, G. Bauer, and S. H. Christiansen, "Roughness of silicon nanowire sidewalls and room temperature photoluminescence," *Physical Review B*, vol. 82, no. 12, Article ID 125446, 2010.

[20] I. Leontis, A. Othonos, and A. G. Nassiopoulou, "Structure, morphology, and photoluminescence of porous Si nanowires: effect of different chemical treatments," *Nanoscale Research Letters*, vol. 8, no. 1, p. 383, 2013.

[21] J. Bullot and M. P. Schmidt, "Physics of amorphous silicon-carbon alloys," *Physica Status Solidi*, vol. 143, no. 2, pp. 345–418, 1987.

[22] K. K. Khichar, S. B. Dangi, V. Dhayal et al., "Structural, optical, and surface morphological studies of ethyl cellulose/graphene oxide nanocomposites," *Polymer Composites*, vol. 41, no. 7, pp. 2792–2802, 2020.

[23] V. Dhayal, S. Z. Hashmi, U. Kumar et al., "Spectroscopic studies, molecular structure optimization and investigation of structural and electrical properties of novel and biodegradable Chitosan-GO polymer nanocomposites," *Journal of Materials Science*, vol. 55, no. 30, pp. 14829–14847, 2020.

[24] A. Ali, Y. W. Chiang, and R. M. Santos, "X-Ray techniques for mineral characterization: a review for engineers of the fundamentals, applications, and research directions," *Minerals*, vol. 12, pp. 1–25, 2022.

[25] I. Minin and O. V. Minin, *Elements of Diffraction Quasi-Optics*, Bridge12 Technologies, Natick, MA, USA, 1994.

[26] E. Lifshim, *X-ray Characterization of Materials*, Wiley, Hoboken, NJ, USA, 1999.

[27] F. Bastianini, G. E. Perez, A. R. Hobson et al., "In–situ monitoring Poly(3-hexylthiophene) nanowire formation and shape evolution in solution via small angle neutron scattering," *Solar Energy Materials and Solar Cells*, vol. 202, Article ID 110128, 2019.

[28] N. A. C. Lah and S. Trigueros, "Synthesis and modelling of the mechanical properties of Ag, Au, and Cu nanowires," *Science and Technology of Advanced Materials*, vol. 20, no. 1, pp. 225–261, 2019.

[29] S. K. Sen, M. M. H. Babu, T. C. Paul et al., "Gamma irradiated nanostructured $NiFe_2O_4$: effect of γ-photon on morphological, structural, optical, and magnetic properties," *AIP Advances*, vol. 11, no. 7, Article ID 075308, 2021.

[30] S. K. Sen, T. C. Paul, S. Dutta, M. A. Matin, M. F. Islam, and M. A. Hakim, "Effect of gamma (γ-) irradiation on the

structural, morphological, optical and electrical properties of spray pyrolysis-deposited h-MoO$_3$ thin films," *Surfaces and Interfaces*, vol. 17, Article ID 100377, 2019.

[31] I. Zardo, L. Yu, S. Conesa-Boj et al., "Gallium assisted plasma enhanced chemical vapor deposition of silicon nanowires," *Nanotechnology*, vol. 20, no. 15, pp. 155602–155609, 2009.

[32] V. Schmidt, J. V. Wittemann, S. Senz, and U. Gösele, "Silicon nanowires: a review on aspects of their growth and their electrical properties," *Advanced Materials*, vol. 21, no. 25-26, pp. 2681–2702, 2009.

[33] T. T. Nguyen, A. X. Vuong, L. D. Mai et al., "Growth of silicon nanowires by sputtering and evaporation methods," *Physica Status Solidi*, vol. 210, no. 7, pp. 1429–1432, 2013.

[34] M. Madani, "Structure, optical and thermal decomposition characters of LDPE graft copolymers synthesized by gamma irradiation," *Bulletin of Materials Science*, vol. 33, no. 1, pp. 65–73, 2010.

[35] L. A. Osminkina, K. A. Gonchar, V. S. Marshov et al., "Optical properties of silicon nanowire arrays formed by metal-assisted chemical etching: evidences for light localization effect," *Nanoscale Research Letters*, vol. 7, no. 1, pp. 524–526, 2012.

[36] S. D. Hutagalung, M. M. Fadhali, R. A. Areshi, and F. D. Tan, "Optical and electrical characteristics of silicon nanowires prepared by electroless etching," *Nanoscale Research Letters*, vol. 12, no. 1, p. 425, 2017.

[37] K. S. Hemalatha, K. Rukmani, N. Suriyamurthy, and B. M. Nagabhushana, "Synthesis, characterization and optical properties of hybrid PVA-ZnO nanocomposite: a composition dependent study," *Materials Research Bulletin*, vol. 51, pp. 438–446, 2014.

[38] S. B. Aziz, O. G. Abdullah, M. A. Brza, A. K. Azawy, and D. A. Tahir, "Effect of carbon nano-dots (CNDs) on structural and optical properties of PMMA polymer composite," *Results in Physics*, vol. 15, Article ID 102776, 2019.

[39] N. D. Baydogan, "Evaluation of optical properties of the amorphous carbon film on fused silica," *Materials Science and Engineering: B*, vol. 107, no. 1, pp. 70–77, 2004.

[40] A. Benmoussa, S. Gissot, U. Schuhle et al., "On-orbit degradation of solar instruments," *Solar Physics*, vol. 288, no. 1, pp. 389–434, 2013.

[41] S. V. Gaponenko, *Optical Properties of Semiconductor Nanocrystals*, Cambridge University Press, Cambridge, UK, 1998.

[42] A. Shik, *Quantum Wells: Physics and Electronics of Two-Dimensional Systems*, World Scientific, Singapore, 1997.